LES OF SPATIAL TRANSITION IN PLANE CHANNEL FLOW

Philipp Schlatter, Steffen Stolz, Leonhard Kleiser
Institute of Fluid Dynamics
Swiss Federal Institute of Technology ETH Zürich
CH-8092 Zürich, Switzerland
schlatter@ifd.mavt.ethz.ch

ABSTRACT

Spatial large-eddy simulations (LES) of forced transition in plane channel flow are presented and compared to temporal simulations. Using the fringe method, spectral Fourier discretisation can be employed also in the streamwise, spatially evolving flow direction. Various subgrid-scale (SGS) models have been examined, including the dynamic Smagorinsky model, high-pass filtered (HPF) eddy-viscosity models and the relaxation term model (ADM-RT). The applicability of the fringe method in conjunction with a SGS model is discussed. It is shown that all SGS models cause a significant improvement of the results over a coarse-grid no-model calculation. The most accurate prediction of transitional flow structures is obtained using the ADM-RT model. The results also show that the SGS models behave similarly in temporal and spatial simulations.

INTRODUCTION

The ability to accurately simulate transitional flows using large-eddy simulation (LES) would greatly improve the usability of LES in many practical industrial applications in which laminar-turbulent transition plays a crucial role, as e.g. flows along airplane wings or in turbomachinery. It has already been shown in a number of publications that the model problem of temporal transition in channel flow can be simulated quite accurately by LES on a much coarser grid than needed for a corresponding fully resolved direct numerical simulation (DNS), see e.g. Germano *et al.* (1991) and Schlatter *et al.* (2004c) and the references therein. Large-eddy simulations of a spatially evolving transitional boundary layer have been presented by Ducros *et al.* (1996) applying successfully the filtered structure-function model. Recently, Schlatter *et al.* (2004a) employed LES with a relaxation regularisation (ADM-RT model, see below) to simulate forced temporal transition. Comparison with DNS (Sandham and Kleiser, 1992) showed a very good prediction of transitional flow structures like the formation of Λ-vortices, hairpin vortices and the roll-up of the shear layers.

The present contribution focuses on extending these studies to spatial transition, in which the disturbances grow in the streamwise direction rather than in time. Whereas the similarity of the spatial and temporal approach is well-established for the early transitional stages and for developed turbulence (Kleiser and Zang, 1991), there are differences during the highly intermittent later transitional stages concerning the physical flow structure and, possibly, the appropriate subgrid-scale (SGS) modelling.

SGS MODELLING

The governing equations for LES are the (spatially) filtered Navier-Stokes equations for the non-dimensional velocity components $\overline{u}_i$ $(i = 1, 2, 3)$ and the pressure $\overline{p}$,

$$\frac{\partial \overline{u}_i}{\partial t} + \frac{\partial \overline{u}_i \overline{u}_j}{\partial x_j} + \frac{\partial \overline{p}}{\partial x_i} - \frac{1}{Re_b} \frac{\partial^2 \overline{u}_i}{\partial x_j \partial x_j} = -\frac{\partial \tau_{ij}}{\partial x_j} + F_i^F \ , \quad (1)$$

complemented with the incompressibility constraint $\partial \overline{u}_i / \partial x_i = 0$. The effect of the non-resolved small scales enters through the SGS term $\tau_{ij} := \overline{u_i u_j} - \overline{u}_j \overline{u}_i$, which is not closed and must be modelled appropriately. The term F_i^F arises from the fringe forcing which will be discussed in the following section.

For the present results, a number of different SGS models have been examined. All of these models have already been tested in temporal K-type transition in plane Poiseuille flow (Schlatter *et al.* (2004c); Stolz *et al.* (2004); Schlatter *et al.* (2004d)) with the same spectral numerical method. In particular, eddy-viscosity models with the ansatz

$$\tau_{ij} - \frac{\delta_{ij}}{3} \tau_{kk} \approx -2 \nu_t S_{ij}(\overline{\mathbf{u}}) \ , \quad (2)$$

and

$$S_{ij}(\overline{\mathbf{u}}) = \frac{1}{2} \left(\frac{\partial \overline{u}_i}{\partial x_j} + \frac{\partial \overline{u}_j}{\partial x_i} \right) \quad (3)$$

are considered. The *dynamic Smagorinsky model* has been implemented according to Germano *et al.* (1991) and Lilly (1992) with a three-dimensional second-order Padé test filter. The eddy-viscosity is then defined as

$$\nu_t = (C_S \Delta)^2 |S(\overline{\mathbf{u}})| \ , \quad (4)$$

with the dynamic model coefficient $C_S(x, z, t)$. The averaging involved in the computation of C_S is performed in the spanwise direction y only and negative values are clipped.

In the *filtered structure function (FSF) model* (Ducros *et al.*, 1996) the eddy-viscosity is given by

$$\nu_t = C_{FSF} C_K^{-3/2} \Delta \sqrt{F_2(H_0 * \overline{\mathbf{u}}, \mathbf{x}, \Delta)} \ , \quad (5)$$

with $C_{FSF} = 0.0371$ (Schlatter *et al.*, 2004b) and the second-order velocity structure function F_2 computed in the three-dimensional 6-point formulation from the high-pass filtered velocity field $H_0 * \overline{u} = (I - G) * \overline{u}$. The definition of the filter G is given in Stolz *et al.* (2001) and its transfer function $\hat{G}$ is shown in figure 1. The cutoff wavenumber ω_c is defined by $\hat{G}(\omega_c) = 1/2$. For the present results, $\omega_c = 2\pi/3$ is used. The filter is defined on an implicit 5-point stencil in physical space, and it is assured that all moments in

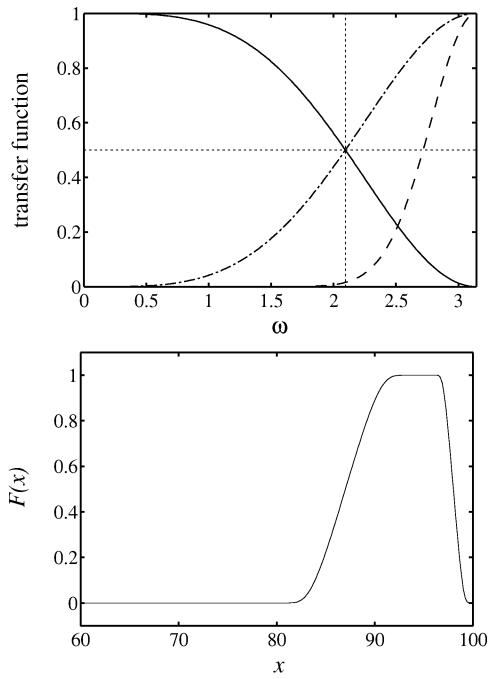

Figure 1: *Top:* Transfer function of the filters used for the SGS models: ——Low-pass filter $\hat{G}$, —·—high-pass filter $\hat{H}_0 = 1 - \hat{G}$, – – – –high-pass filter $\hat{H}_5 = (1 - \hat{G})^6$. Cutoff wavenumber $\omega_c = 2\pi/3$. *Bottom:* Fringe function $F(x)$ on the subdomain $[60, 100]$.

physical space up to second order are vanishing even for non-equidistant grids, as e.g. used in the the wall-normal direction of the channel. For this reason smooth (i.e. low-order polynomial) flow profiles are virtually invariant with respect to the filter operation and are thus small when high-pass filtered with $H_N := (I - G)^{N+1},\ N \geq 0$.

In contrast to classical eddy-viscosity models, the *high-pass filtered (HPF) eddy-viscosity models* (Stolz *et al.*, 2004) compute both the strain-rate and the eddy-viscosity from the high-pass filtered velocities, i.e.

$$\tau_{ij} - \frac{\delta_{ij}}{3}\tau_{kk} \approx -2\nu_t^{\mathrm{HPF}} S_{ij}(H_0 * \overline{\mathbf{u}}) \ , \tag{6}$$

with the corresponding eddy-viscosity (HPF-SF model)

$$\nu_t^{\mathrm{HPF}} = C_{SF}^{\mathrm{HPF}} C_K^{-3/2} \Delta \sqrt{F_2(H_0 * \overline{\mathbf{u}}, \mathbf{x}, \Delta)} \ , \tag{7}$$

and $C_{SF}^{\mathrm{HPF}} = 0.0405$ (Schlatter *et al.*, 2004b).

The *ADM-RT model* is based on the relaxation term (RT) of the approximate deconvolution model (ADM) (Stolz *et al.*, 2001) presented in Stolz and Adams (2003) and Schlatter *et al.* (2004c,d), where a regularisation term $\chi H_5 * \overline{u}_i$ is employed in the momentum equations (1),

$$\frac{\partial \tau_{ij}}{\partial x_j} = \chi H_5 * \overline{u}_i \ . \tag{8}$$

Here, $H_5 = (I - G)^6$ denotes the high-order three-dimensional high-pass filter (Stolz *et al.*, 2001) respecting the boundary conditions, see figure 1. χ is a model coefficient, which is set to a constant value herein. The ADM-RT model proved to be accurate and robust in predicting transitional and turbulent incompressible flows with spectral methods (Schlatter *et al.*, 2004c,d).

NUMERICAL METHOD, BOUNDARY TREATMENT, AND PARAMETER SETTINGS

The simulations use a standard Fourier-Chebyshev spectral method with periodic boundary conditions in the streamwise (x) and spanwise (y) directions together with no-slip conditions at the solid walls ($z = \pm 1$). The nonlinear convection terms are computed with full dealiasing employing the 3/2-rule in all spatial directions. No dealiasing has been used for the SGS model terms. The divergence-free condition is enforced exactly by an influence-matrix technique (Kleiser and Schumann, 1980). Time advancement is achieved by a semi-implicit Runge-Kutta/Crank-Nicolson scheme of third order (Sandham and Kleiser, 1992).

To account for the spatially evolving flow a fringe region has been added to the flow domain in the streamwise direction similar to Bertolotti *et al.* (1992) and Nordström *et al.* (1999). Within this region, which accounts for 20% of the streamwise extent of the computational domain, the term

$$F_i^F = \lambda(x)(\mathcal{U}_i - \overline{u}_i) \tag{9}$$

in equation (1) forces the flow to return from the outflow profile back to the prescribed inflow profile $\mathcal{U}_i$. The fringe function is defined as $\lambda(x) = \lambda_f \cdot F(x)$ with $F(x)$ given by Nordström *et al.* (1999),

$$F(x) = S\left(\frac{x - x_{\mathrm{start}}}{\Delta_{\mathrm{rise}}}\right) - S\left(\frac{x - x_{\mathrm{end}}}{\Delta_{\mathrm{fall}}} + 1\right) \ , \tag{10}$$

with the smooth step function

$$S(x) \quad = \quad \begin{cases} 0 & , \ x \leq 0 \\ 1/[1 + \exp(\frac{1}{x-1} + \frac{1}{x})] & , \ 0 < x < 1 \\ 1 & , \ x \geq 1 \end{cases} . \tag{11}$$

The fringe function $\lambda(x) \geq 0$ and thus the forcing term F_i^F is non-vanishing only within the fringe region extending from $x_{\mathrm{start}} = 80$ to $x_{\mathrm{end}} = 100$ for the present investigation. The shape of the fringe function is further defined by $\Delta_{\mathrm{rise}} = 14$ and $\Delta_{\mathrm{fall}} = 4$ (see figure 1).

The inflowing disturbances are superimposed onto the laminar Poiseuille flow and forced within the fringe region as distributed boundary conditions $\overline{u}_i \leftarrow \mathcal{U}_i(x, y, z, t)$. They consist of a two-dimensional spatially evolving Tollmien-Schlichting (TS) wave and two superimposed oblique three-dimensional waves with the same temporal frequency $\omega_{TS} = 0.3$ as the two-dimensional disturbances. The amplitude of these disturbances is set to 6% and 0.2%, respectively, being twice as high as the temporal reference simulation of Gilbert and Kleiser (1990) and Schlatter *et al.* (2004c) in order to trigger transition earlier and thus to allow for a shorter computational domain. These initial conditions excite standard K-type transition with an aligned pattern of Λ-vortices. The Reynolds number based on the bulk velocity and the channel half-width h is $Re_b = 3333$ (corresponding to $Re_\tau \approx 210$ in the fully turbulent regime). Statistical data has been averaged in y and in time from $t = 200$ to $t = 410$, corresponding to 10 periods of the initial TS wave. The dimensions of the computational box are $100h \times 3h \times 2h$. An overview of the flow development within the computational box is shown in figure 2.

RESULTS

As a first step, the application of the fringe method to the LES equations using a SGS model has to be examined. Several

Figure 2: Visualisation of the solution (λ_2) within the entire computational domain in a x, y-plane. The inflow is located on the left, whereas the fringe domain $80 \leq x \leq 100$ is appended on the right-hand side (see also figure 1).

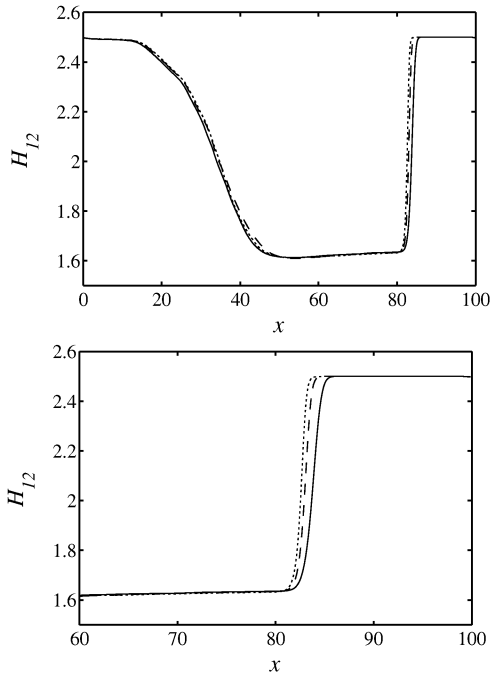

Figure 3: Evolution of the shape factor H_{12} during transition using ADM-RT on $768 \times 48 \times 49$ grid points, $\chi = 25$. ——— $\lambda_f = 10$, - - - - $\lambda_f = 40$, ····· $\lambda_f = 100$. *Top:* Full domain. *Bottom:* Enlargement of the fringe region.

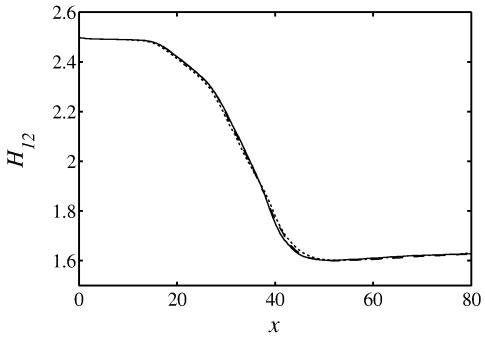

Figure 4: Evolution of the shape factor H_{12} during transition using ADM-RT on $512 \times 32 \times 33$ grid points. ——— $\chi = 25$, $\lambda_f = 40$, - - - - $\chi = 50$, $\lambda_f = 40$, —·— $\chi = 25$, $\lambda_f = 10$.

LES using the ADM-RT model have been performed varying both the fringe strength λ_f and the relaxation parameter χ. In figure 3, three simulations on a $768 \times 48 \times 49$ grid are compared for which λ_f was varied by a factor of up to 10 with fixed $\chi = 25$. In the physically relevant subdomain $x \in [0, 80]$, the shape factor H_{12} nearly collapses for the different runs, whereas in the fringe region $x > 80$ a higher λ_f reestablishes the laminar profile earlier, $H_{12} \approx 2.5$. At a lower resolution of $512 \times 32 \times 33$ grid points, figure 4 displays H_{12} for different combinations of χ and λ_f, again showing no significant discrepancies. Additionally, tests have been conducted with

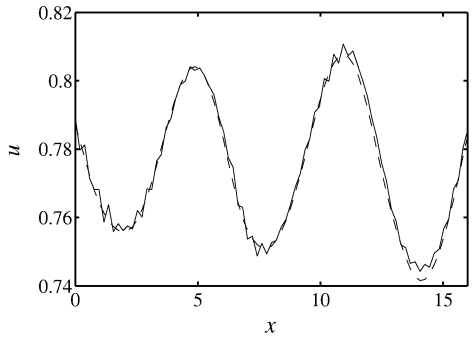

Figure 5: Streamwise velocity $\overline{u}$ close to the inflow at $z = -0.47$ computed using - - - - ADM-RT and ——— no-model LES on $512 \times 32 \times 33$ grid points.

gradually reducing the influence of the SGS model within the fringe region by setting $\partial \tau_{ij} / \partial x_j = (1 - F(x)) \chi H_5 * \overline{u}_i$. It was found that such a modification was not necessary for an accurate prescription of the inflow conditions.

On the other hand, the application of the fringe method without any SGS model (no-model LES) at the low LES resolution ($512 \times 32 \times 33$ nodes) caused the appearance of small wiggles in the instantaneous velocity as shown in figure 5. These wiggles are not present if a SGS model is used at the same resolution. They are most likely caused by the underresolution in the later stages of transition and in the turbulent part of the flow domain. Due to the global discretisation scheme the wiggles are able to affect the whole flow domain. By increasing the resolution, these artefacts are reduced gradually and eventually vanish as soon as sufficient resolution is reached in the turbulent part of the domain. Conversely, in the LES these wiggles do not exist even at low resolution since they are effectively damped by the SGS model.

It can thus be concluded that the fringe method provides an efficient and accurate way to enforce inflow and outflow boundary conditions also in the presence of a SGS model. Moreover, it can be seen that the ADM-RT model is not very sensitive to the choice of the model coefficient χ (see also Schlatter *et al.* (2004d) and Stolz *et al.* (2001)).

Transitional Phase

In figure 6 the evolution of the Reynolds number based on the friction velocity Re_τ and the shape factor H_{12} during transition from the slightly disturbed laminar flow to the turbulent state is shown for both the spatial and the temporal framework. The various spatial LES have been performed with a resolution of $512 \times 32 \times 33$ grid points, which corresponds to $32 \times 32 \times 33$ points for one period of the initial TS waves, similar to the temporal LES (Schlatter *et al.*, 2004c; Stolz *et al.*, 2004). It can be seen from the figure that all LES are able to predict transition to turbulence. Compared to the LES with an active SGS model and to the temporal DNS data, the no-model calculation undergoes transition somewhat too early in both the temporal and the spatial simulation. At this resolution the no-model calculation is clearly underresolved,

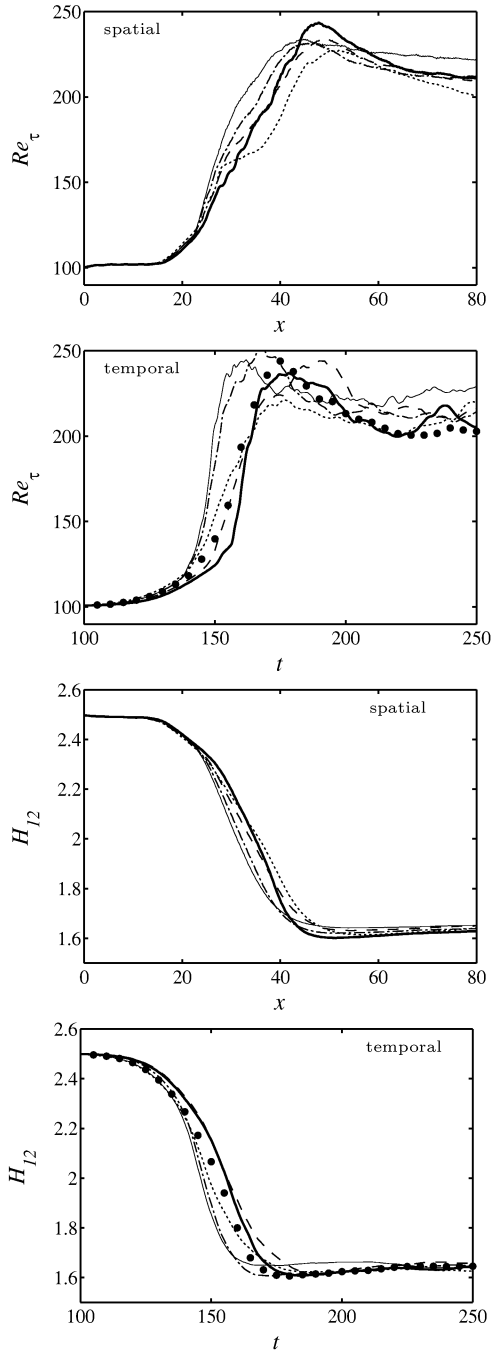

Figure 6: Evolution of the skin friction Reynolds number Re_τ and shape factor H_{12} during transition computed on $512\times32\times33$ grid points in the spatial framework ($\lambda_f = 40$) and in the temporal framework on $32\times32\times33$ grid points. ——— ADM-RT model with $\chi = 25$, ····· dynamic Smagorinsky model, – – – – FSF model, –·– HPF-SF model, ——— no-model LES, • temporal DNS (resolution $160\times160\times161$ grid points).

which can also be seen in visualisations of the instantaneous fields showing small wiggles in the velocities (see previous section and figure 5). The qualitative behaviour of the different models is quite comparable between the temporal and spatial approach; i.e. the FSF model closely follows the no-model LES at lower x (earlier times in temporal LES), and during later

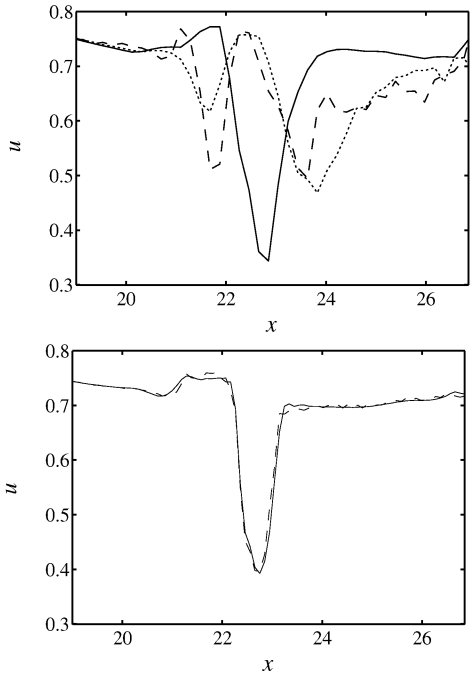

Figure 7: Streamwise velocity $\overline{u}$ for the one-spike stage at $z = -0.47$. *Top:* Resolution $512\times32\times33$, ——— ADM-RT, ····· dynamic Smagorinsky model, – – – – no-model LES. *Bottom:* Resolution $1024\times64\times65$, ——— high-resolution ADM-RT, – – – – no-model LES (low-resolution spatial DNS).

stages it seems to be too dissipative. The same conclusion can be drawn for the dynamic Smagorinsky model, which however provides a more accurate description of the earlier transitional stages. It is interesting to note that in the spatial simulations the typical overshoot of Re_τ during transition is predicted only by the ADM-RT model with similar amplitude (ca. 15%) as in the temporal DNS and the corresponding temporal LES.

Transitional Structures

Instantaneous velocity signals are displayed in figures 7 and 9 showing the typical low-velocity "spike" stages associated with the transitional breakdown (Nishioka *et al.*, 1975; Gilbert and Kleiser, 1990). From figure 7 it can be inferred that the one-spike stage is predicted accurately only by the ADM-RT model at the present low resolution. Both the no-model simulation and the data of the dynamic Smagorinsky model do not show this distinct early transitional stage at any time, which is associated with the appearance of the first hairpin vortex. However, by doubling the resolution to $1024\times64\times65$ grid points, the one-spike stage becomes also visible in the no-model data (low-resolution DNS), nearly collapsing with the ADM-RT data.

For the ADM-RT model, the sequence of velocity signals from the one-spike to the four-spike stage is shown in figure 9. All stages can be clearly identified and are qualitatively similar to those obtained by either temporal or spatial simulations at higher resolutions (Sandham and Kleiser, 1992; Schlatter *et al.*, 2004a).

A visualisation of the instantaneous flow field by means of the negative-λ_2 vortex-identification criterion (Jeong and Hussain, 1995) is presented in figure 8 for some SGS models and resolutions at the two-spike stage. For all models,

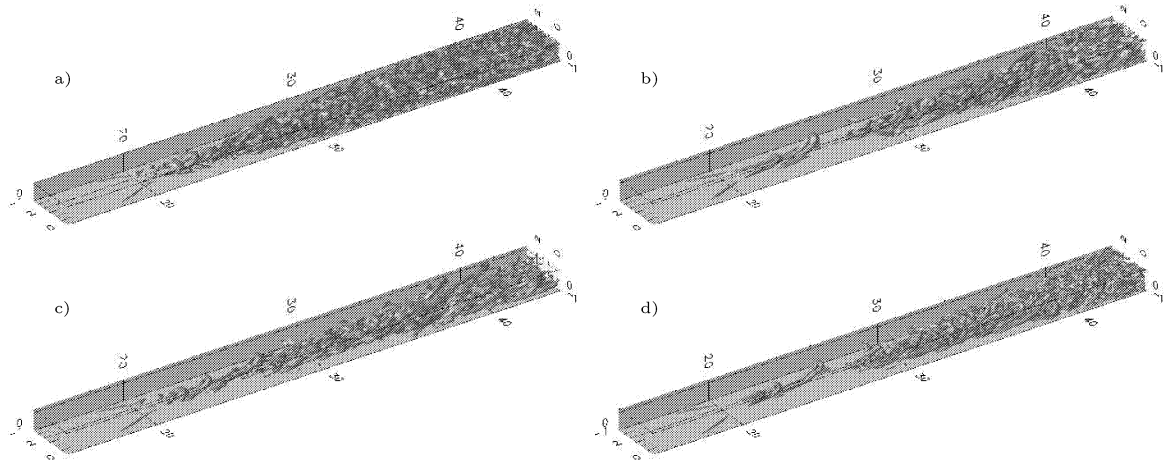

Figure 8: Visualisation of the instantaneous vortical structures at the two-spike stage on $512 \times 32 \times 33$ grid. (a) No-model LES, (b) ADM-RT model, (c) dynamic Smagorinsky model, (d) ADM-RT model on $1024 \times 64 \times 65$ grid (high-resolution LES).

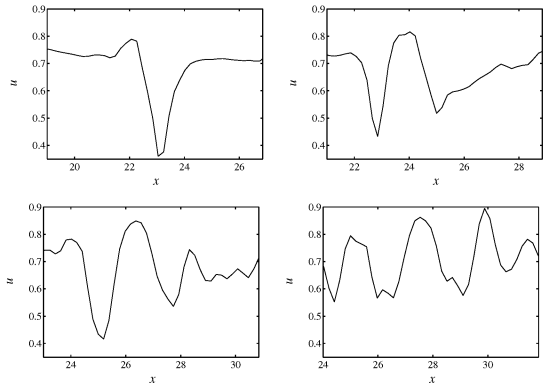

Figure 9: Streamwise velocity $\overline{u}$ for the various spike stages at $z = -0.47$ computed using ADM-RT on $512 \times 32 \times 33$ grid points. The streamwise extent of the plotted region corresponds to the streamwise wavelength of the TS wave. From left to right and top to bottom: one-spike stage, $t^* = 0$, two-spike stage, $t^* = 4$, three-spike stage, $t^* = 8$, four-spike stage, $t^* = 10$ (t^* relative time).

the remainders (legs) of the Λ-vortices are visible at $x \approx 19$. The no-model data does not show the two typical hairpin vortices expected at this stage of development, and the flow field breaks down to turbulence too fast without the appearance of these distinct vortical structures. The data obtained with the ADM-RT model for both resolutions shows distinct hairpin vortices with comparable downstream evolution of the structures and spreading of the turbulent region from the peak plane ($y = L_y/2$) towards the lateral boundaries of the domain. The dynamic Smagorinsky model also features some of these structures, however they are not as distinct as for the ADM-RT model. Especially further downstream ($x \approx 35$) the former model is too dissipative as indicated by an apparently coarser vortical structure present in the data. Note that with the chosen low LES resolution the spanwise extent of the hairpin vortex is resolved by approximately 5 grid points only.

Turbulent Channel Flow

To confirm the accuracy of the LES in the turbulent stage, the spanwise and temporally averaged mean velocity profiles and Reynolds stresses are shown in figure 10 for the downstream position $x = 77$ close to the fringe region (which begins at $x = 80$). As a reference, the corresponding data obtained from the temporal simulations are also shown. Although turbulence is not yet fully developed at that position, a close agreement between the temporal DNS and the ADM-RT model can be observed. Moreover, the same qualitative behaviour for the Reynolds stresses and the mean streamwise velocity profile can be established for the various LES data obtained from the spatial and temporal simulations (Stolz *et al.*, 2004; Schlatter *et al.*, 2004c).

CONCLUSIONS

In this work, LES of spatial transition in plane channel flow using the fringe method and various SGS models have been presented. The results suggest that LES, in particular when using the ADM relaxation term model, shows substantial improvement over no-model (underresolved DNS) computation for both the prediction of the transition process as well as for the turbulent statistics. Instantaneous vortical structures (e.g. hairpin vortices) are also predicted well by the LES even on a rather coarse grid. However, the different spike stages are predicted correctly in detail only by the ADM-RT model. The combination of LES with the fringe method did not raise any difficulties even with a SGS model active within the fringe region.

It has also been shown that the different SGS models examined in this contribution behave similarly for both the temporal and the spatial simulation approach. Conclusions based on temporal results therefore transfer readily to the spatial simulation method, which is more physically realistic but also much more computationally expensive.

ACKNOWLEDGMENTS

This work was supported by the Swiss National Science Foundation (SNF) and the Swiss National Supercomputing Centre (CSCS). Calculations have been performed at CSCS.

REFERENCES

Bertolotti, F. P., Herbert, T., and Spalart, P. R., 1992. "Linear and nonlinear stability of the Blasius boundary layer." *J. Fluid Mech.*, vol. 242, pp. 441–474.

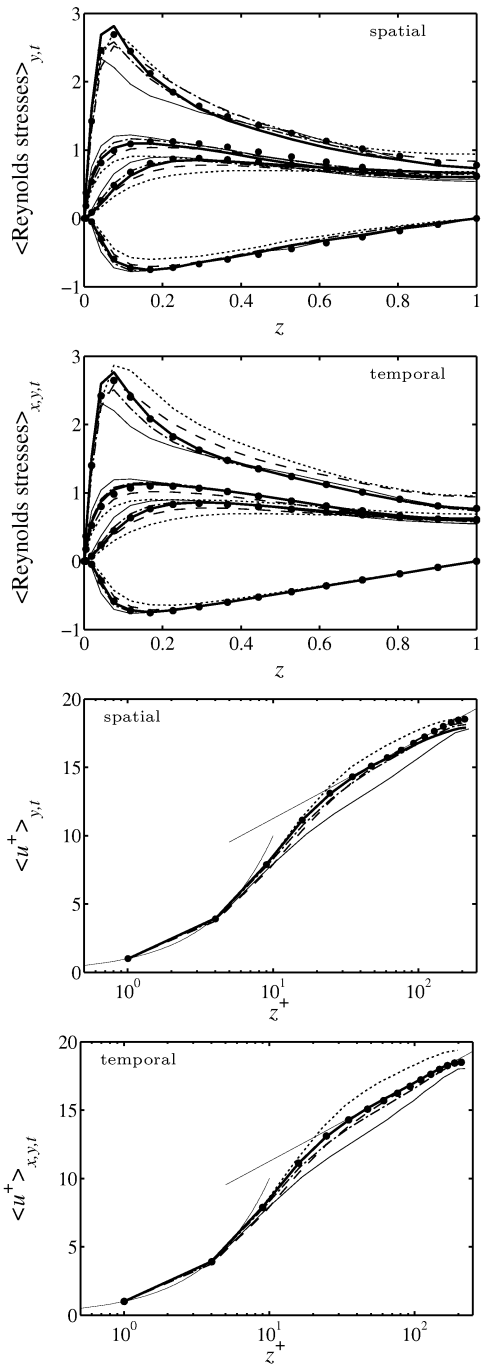

Figure 10: Averaged turbulent statistics: Reynolds stresses $\langle \overline{u}_1' \overline{u}_1' \rangle^{1/2}/u_\tau$, $\langle \overline{u}_2' \overline{u}_2' \rangle^{1/2}/u_\tau$, $\langle \overline{u}_3' \overline{u}_3' \rangle^{1/2}/u_\tau$, $\langle \overline{u}_1' \overline{u}_3' \rangle/u_\tau^2$ and the mean streamwise velocity profile $\overline{u}^+$ in wall units computed on $512 \times 32 \times 33$ grid in the spatial framework ($\lambda_f = 40$) and on $32 \times 32 \times 33$ grid in the temporal framework. ——— ADM-RT model with $\chi = 25$, ····· dynamic Smagorinsky model, – – – – FSF model, —·— HPF-SF model, ——— no-model LES, • temporal DNS (resolution $160 \times 160 \times 161$).

Ducros, F., Comte, P., and Lesieur, M., 1996. "Large-eddy simulation of transition to turbulence in a boundary layer developing spatially over a flat plate." *J. Fluid Mech.*, vol. 326, pp. 1–36.

Germano, M., Piomelli, U., Moin, P., and Cabot, W. H., 1991. "A dynamic subgrid-scale eddy viscosity model." *Phys. Fluids A*, vol. 3(7), pp. 1760–1765.

Gilbert, N. and Kleiser, L., 1990. "Near-wall phenomena in transition to turbulence." In Kline, S. J. and Afgan, N. H., eds., *Near-Wall Turbulence – 1988 Zoran Zarić Memorial Conference*, pp. 7–27. Hemisphere, New York, USA.

Jeong, J. and Hussain, F., 1995. "On the identification of a vortex." *J. Fluid Mech.*, vol. 285, pp. 69–94.

Kleiser, L. and Schumann, U., 1980. "Treatment of incompressibility and boundary conditions in 3-D numerical spectral simulations of plane channel flow." In Hirschel, E. H., ed., *Proc. 3rd GAMM Conf. on Numerical Methods in Fluid Mechanics*, pp. 165–173. Vieweg, Braunschweig, Germany.

Kleiser, L. and Zang, T. A., 1991. "Numerical simulation of transition in wall-bounded shear flows." *Annu. Rev. Fluid Mech.*, vol. 23, pp. 495–537.

Lilly, D. K., 1992. "A proposed modification of the Germano subgrid-scale closure method." *Phys. Fluids A*, vol. 4(3), pp. 633–635.

Nishioka, M., Iida, S., and Ichikawa, Y., 1975. "An experimental investigation of the stability of plane Poiseuille flow." *J. Fluid Mech.*, vol. 72, pp. 731–751.

Nordström, J., Nordin, N., and Henningson, D. S., 1999. "The fringe region technique and the Fourier method used in the direct numerical simulation of spatially evolving viscous flows." *SIAM J. Sci. Comput.*, vol. 20(4), pp. 1365–1393.

Sandham, N. D. and Kleiser, L., 1992. "The late stages of transition to turbulence in channel flow." *J. Fluid Mech.*, vol. 245, pp. 319–348.

Schlatter, P., Stolz, S., and Kleiser, L., 2004a. "Applicability of LES models for prediction of transitional flow structures." In *IUTAM Symposium on Laminar-Turbulent Transition*. To appear.

Schlatter, P., Stolz, S., and Kleiser, L., 2004b. "High-pass filtered eddy-viscosity models in incompressible high-Reynolds number flows." In Andersson, H. I. and Krogstad, P.-Å., eds., *Advances in Turbulence X*, pp. 303–306. CIMNE, Barcelona, Spain.

Schlatter, P., Stolz, S., and Kleiser, L., 2004c. "LES of transitional flows using the approximate deconvolution model." *Int. J. Heat Fluid Flow*, vol. 25(3), pp. 549–558.

Schlatter, P., Stolz, S., and Kleiser, L., 2004d. "Relaxation-term models for LES of transitional/turbulent flows and the effect of aliasing errors." In Friedrich, R., Geurts, B. J., and Métais, O., eds., *Direct and Large-Eddy Simulation V*, pp. 65–72. Kluwer, Dordrecht, The Netherlands.

Stolz, S. and Adams, N. A., 2003. "Large-eddy simulation of high-Reynolds-number supersonic boundary layers using the approximate deconvolution model and a rescaling and recycling technique." *Phys. Fluids*, vol. 15(8), pp. 2398–2412.

Stolz, S., Adams, N. A., and Kleiser, L., 2001. "An approximate deconvolution model for large-eddy simulation with application to incompressible wall-bounded flows." *Phys. Fluids*, vol. 13(4), pp. 997–1015.

Stolz, S., Schlatter, P., Meyer, D., and Kleiser, L., 2004. "High-pass filtered eddy-viscosity models for LES." In Friedrich, R., Geurts, B. J., and Métais, O., eds., *Direct and Large-Eddy Simulation V*, pp. 81–88. Kluwer, Dordrecht, The Netherlands.